

Observations of relativistic electron precipitation due to combined scattering of whistler-mode and EMIC waves

Muhammad Fraz Bashir¹, Anton V Artemyev², Xiao-Jia Zhang³, Vassilis Angelopoulos¹, Ethan Tsai⁴, and Colin Wilkins⁵

¹University of California Los Angeles

²UCLA IGPP

³The University of Texas at Dallas

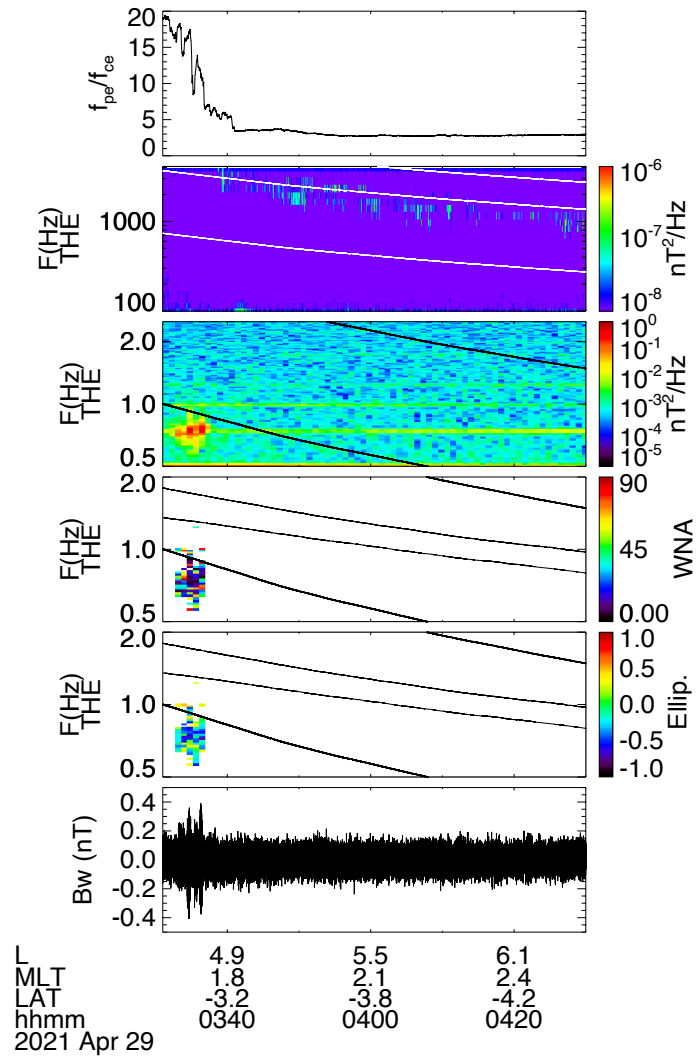
⁴UCLA

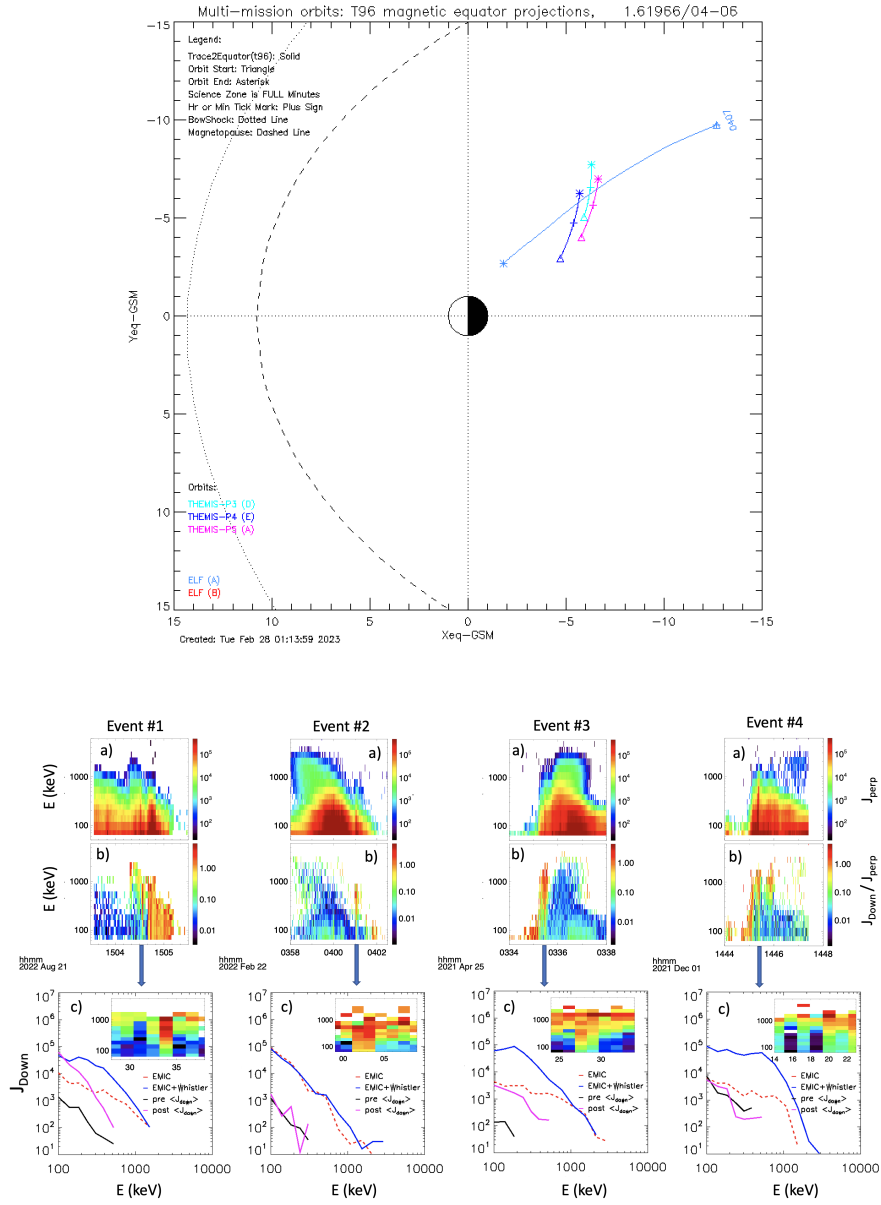
⁵University of California, Los Angeles

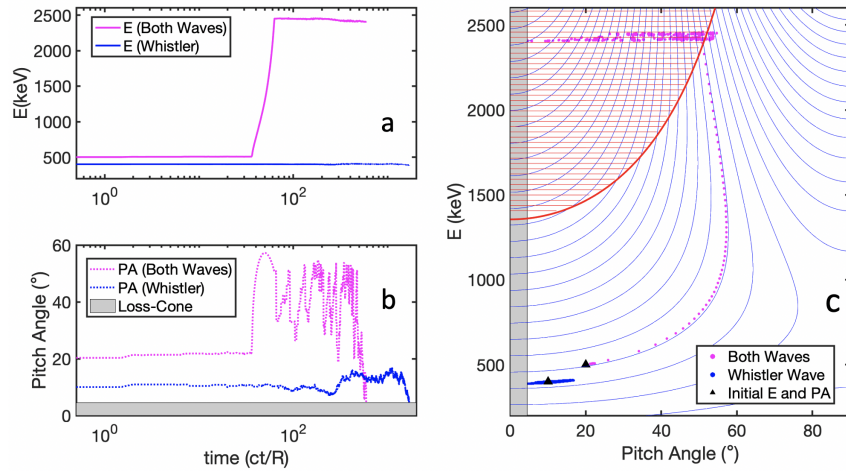
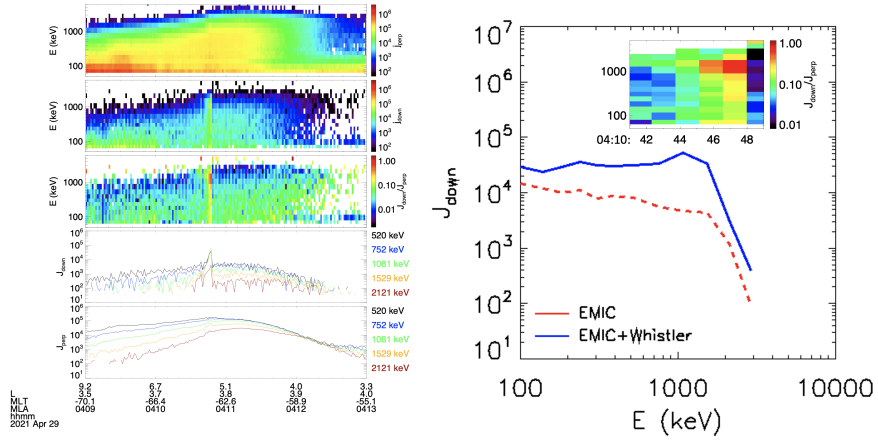
August 4, 2023

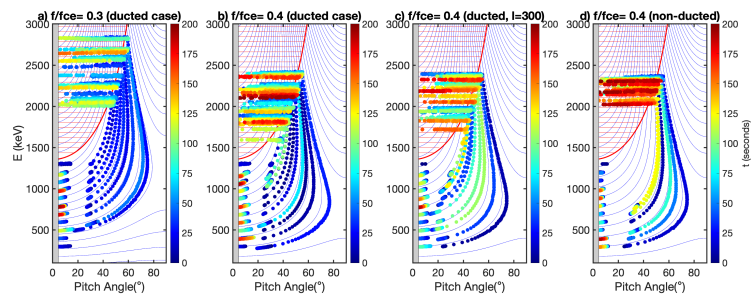
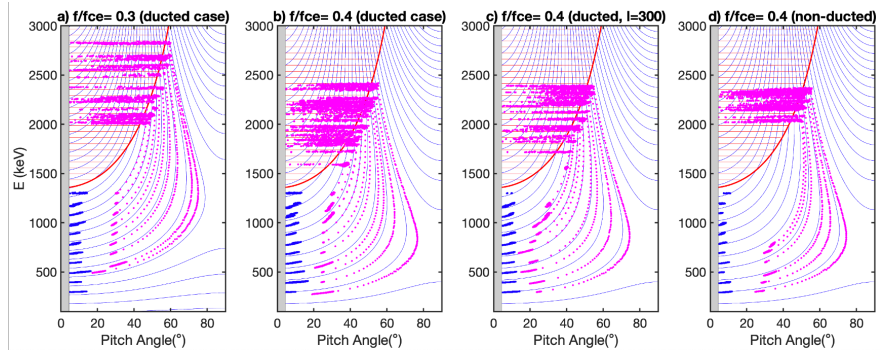
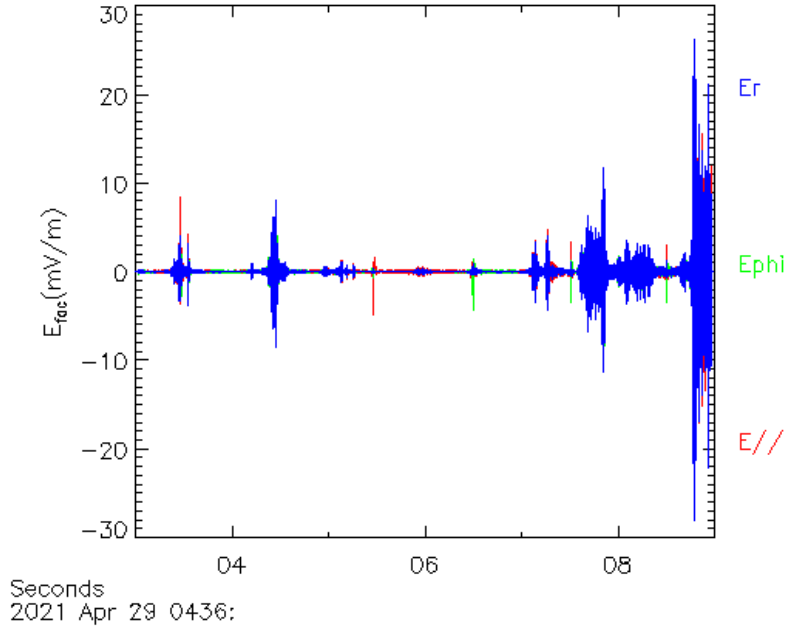
Abstract

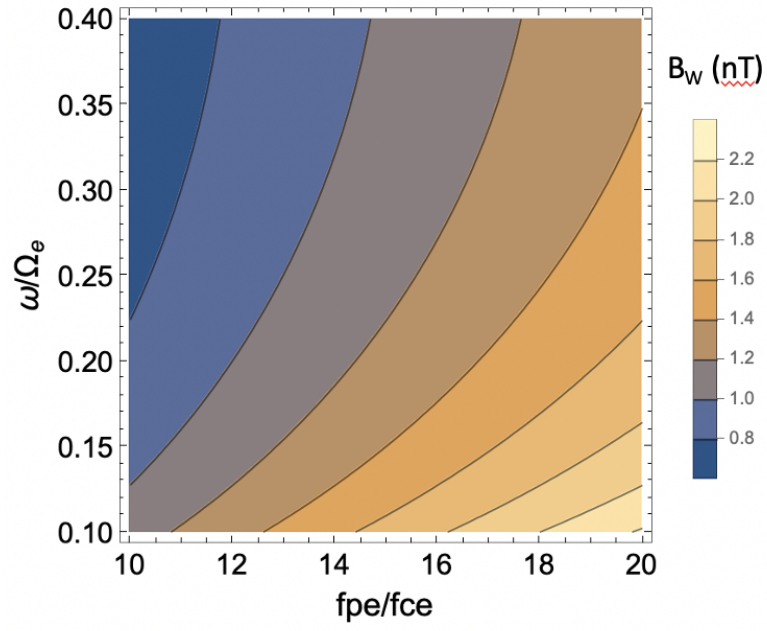
The two most important wave modes responsible for energetic electron scattering to the Earth's ionosphere are electromagnetic ion cyclotron (EMIC) waves and whistler-mode waves. In this study, we report direct observations of energetic electron (from 50 keV to 2.5 MeV) scattering driven by the combined effect of whistler-mode and EMIC waves using ELFIN measurements. We analyze several events exhibiting such properties, and show that electron resonant interactions with whistler-mode waves may enhance relativistic electron precipitation by EMIC waves. During a prototypical event which benefits from conjugate THEMIS measurements, we demonstrate that below the minimum resonance energy (E_{\min}) of EMIC waves, the whistler-mode wave may both scatter electrons into the loss-cone and also accelerate them to higher energy (1-3 MeV). These accelerated electrons above E_{\min} resonate with EMIC waves that, in turn, quickly scatter those electrons into the loss-cone. This enhances relativistic electron precipitation beyond what EMIC waves alone could achieve.











1 **Observations of relativistic electron precipitation due**
2 **to combined scattering of whistler-mode and EMIC**
3 **waves**

4 **M. Fraz Bashir**¹, **Anton Artemyev**^{1,2}, **Xiao-Jia Zhang**^{3,1}, **Vassilis**
5 **Angelopoulos**¹, **E. Tsai**¹, and **C. Wilkins**¹

6 ¹Earth, Planetary, and Space Sciences, University of California, Los Angeles, Los Angeles, CA 90095,
7 USA

8 ²Space Research Institute, RAS, Moscow, Russia

9 ³Department of Physics, University of Texas at Dallas, Richardson, TX, USA

10 **Key Points:**

- 11 • We report observations of energetic electron precipitation likely driven by concur-
12 rent whistler-mode and EMIC waves
- 13 • The combined scattering of whistler-mode and EMIC waves leads to electron pre-
14 cipitation over a wide energy range of 50 keVs to a few MeVs
- 15 • This study highlights the importance of nonlinear effects for explaining the ob-
16 served energetic electron fluxes in the inner magnetosphere

Abstract

The two most important wave modes responsible for energetic electron scattering to the Earth's ionosphere are electromagnetic ion cyclotron (EMIC) waves and whistler-mode waves. In this study, we report the direct observations of energetic electron (from 50 keV to 2.5 MeV) scattering driven by the combined effect of whistler-mode and EMIC waves using ELFIN measurements. We analyze several events exhibiting such properties, and show that electron resonant interactions with whistler-mode waves may enhance relativistic electron precipitation by EMIC waves. During a prototypical event which benefits from conjugate THEMIS measurements, we demonstrate that below the minimum resonance energy (E_{min}) of EMIC waves, the whistler-mode wave may both scatter electrons into the loss-cone and also accelerate them to higher energy (1-3 MeV). These accelerated electrons above E_{min} resonate with EMIC waves that, in turn, quickly scatter those electrons into the loss-cone. This enhances relativistic electron precipitation beyond what EMIC waves alone could achieve.

Plain Language Summary

Energetic electron precipitation into the upper atmosphere is an important loss process of the Earth's inner magnetosphere. Whistler-mode and electromagnetic ion cyclotron (EMIC) waves are the two most important wave modes responsible for energetic electron scattering to the Earth's ionosphere through wave-particle interaction. Although these wave modes typically drive electron losses of different energy ranges (above 1 MeV for EMIC waves and tens to hundreds of keV for whistler-mode waves), the loss mechanism due to the combined effects of EMIC and whistler-mode waves is not well-understood. We report the first direct observation of energetic electron scattering driven by the combined effect of whistler-mode and EMIC waves. Our results from equatorial and low-altitude observations, and from a data-driven test particle simulation explain the wide energy range of electron precipitation from tens of keVs to a few MeVs due to the combined whistler-mode and EMIC waves effect.

1 Introduction

Electromagnetic ion cyclotron (EMIC) and whistler-mode waves are the two main wave modes responsible for energetic electron scattering and precipitation from the Earth's radiation belts into the atmosphere (see reviews by Millan & Thorne, 2007; Li & Hudson, 2019; Thorne et al., 2021). EMIC waves are mostly responsible for the precipitation of relativistic ($> 1\text{MeV}$) electrons (e.g., Usanova et al., 2014; Blum et al., 2015; Shprits et al., 2016, 2017; Ni et al., 2015; Grach & Demekhov, 2020; Bashir & Ilie, 2018, 2021; Bashir et al., 2022b; Capannolo et al., 2018, 2022), whereas whistler-mode waves are very effective in precipitating sub-MeV electrons (see, e.g., reviews by Shprits et al., 2008; Ni et al., 2016; Artemyev et al., 2016; Thorne et al., 2021). Resonant scattering of relativistic ($> 1\text{MeV}$) electrons by whistler-mode waves is most effective at higher electron pitch-angles, which may not result in precipitation (e.g., Summers & Omura, 2007). However, the combined effect of EMIC and whistler-mode waves may enable a rapid decrease of relativistic electron fluxes: whistler-mode waves scatter electrons at higher pitch-angles toward the lower pitch-angle range, where resonance with EMIC waves may quickly scatter these electrons into the loss-cone (e.g., Mourenas et al., 2016; Zhang et al., 2017; Bashir et al., 2022a). Therefore, relativistic electron losses by combined EMIC and whistler-mode wave scattering may critically control the radiation belt dynamics (Drozdov et al., 2020). However, in contrast to electron resonance with EMIC waves providing only pitch-angle scattering (e.g., Summers & Thorne, 2003), resonance with whistler-mode waves can result in both pitch-angle and energy (acceleration) scattering (e.g., Summers, 2005; Glauert & Horne, 2005). If such acceleration is sufficiently fast and efficient, EMIC waves may scatter the newly formed relativistic electron population, those accelerated by whistler-

mode waves, into the loss cone (see discussion in Bashir et al., 2022a). Such precipitation may not require preexisting relativistic electron fluxes, and would not lead to the decrease of preexisting, e.g., previously stably trapped, relativistic electron fluxes. This study combines near-equatorial wave measurements and low-altitude electron precipitation measurements to provide direct evidence for this process in the radiation belts.

To provide a new population of relativistic electrons for subsequent EMIC-driven scattering, electron acceleration by whistler-mode waves should be sufficiently fast. The quasi-linear diffusion rates for average wave intensities show that pitch-angle scattering by EMIC waves is much faster than acceleration by whistler-mode waves (see, e.g., Glauert & Horne, 2005; Summers et al., 2007b). However, very intense whistler-mode waves may resonate with electrons nonlinearly and lead to the rapid formation of relativistic electrons via phase trapping into the turning acceleration (see Omura et al., 2007; Summers & Omura, 2007; Hsieh & Omura, 2017; Hsieh et al., 2020; Bashir et al., 2022a). The rate of this acceleration mechanism may approach the rate of pitch-angle diffusion by EMIC waves, and thus can potentially provide rapid electron acceleration and subsequent losses. In contrast to the simple phase trapping acceleration associated with pitch-angle increase (e.g., Bortnik et al., 2008; Vainchtein et al., 2018), turning acceleration will lead to a pitch-angle decrease with energy increase (Omura et al., 2007), i.e., accelerated particles are transported toward the loss-cone where EMIC waves will scatter them. Thus, additionally to the analysis of electron precipitation events with the combined effect of EMIC and whistler-mode waves, we will focus on a case study with equatorial observations of very intense whistler-mode waves simultaneously observed with EMIC waves.

We use equatorial wave measurements from THEMIS (Angelopoulos, 2008) and low-altitude precipitation measurements from ELFIN (Angelopoulos et al., 2020) to investigate the effect of electron resonant acceleration by whistler-mode waves and the subsequent scattering into the atmosphere by EMIC waves. Section 2 provides an overview of four ELFIN events exhibiting clear signatures of the combined operation of whistler-mode and EMIC waves, Section 3 describes in detail one event benefiting from ELFIN and THEMIS conjunction observations whereas Section 4 discusses possible mechanisms responsible for the enhanced precipitation of relativistic electrons in the simultaneous presence of EMIC and whistler-mode waves. Section 5 summarizes our main findings.

2 ELFIN Observations of Relativistic Electron Precipitation

We use data from the ELFIN-A CubeSat which is equipped with energetic electron detector measuring 50 keV to 6 MeV electrons with an energy resolution of $\Delta E/E < 40\%$ and covering the full (180°) pitch angle twice over a 3 s spin period. Because of its high energy resolution, ELFIN can distinguish precipitation events driven by whistler-mode waves or by EMIC waves (Grach et al., 2022; An et al., 2022; Tsai et al., 2022; Zhang et al., 2022; Angelopoulos et al., 2023). Thus, we focus on putative combined precipitation events which demonstrate properties of both whistler-mode and EMIC wave-driven precipitation.

Figure 1 shows four ELFIN orbits with signatures of electron precipitation due to EMIC and whistler-mode waves. The typical minimum resonance energy for EMIC waves is $\sim 0.5\text{--}1\text{MeV}$ (Summers et al., 2007a; Kersten et al., 2014), so only the part of precipitation above a certain energy should be interpreted as evidence of EMIC-driven precipitation (see the detailed analysis of such events in Angelopoulos et al., 2023). Typical minimum resonance energy for whistler-mode waves (low band chorus waves) is below 10keV (Ni et al., 2012), whereas the scattering rate of electrons by whistler-mode waves decreases with increasing energy (Summers et al., 2007a). Thus, ELFIN observations of precipitation bursts with precipitating-to-trapped flux ratio maximizing at low energies should be interpreted as evidence of whistler-mode wave-driven precipitation (see the detailed analysis of such events in Tsai et al., 2022; Zhang et al., 2022). Mid-

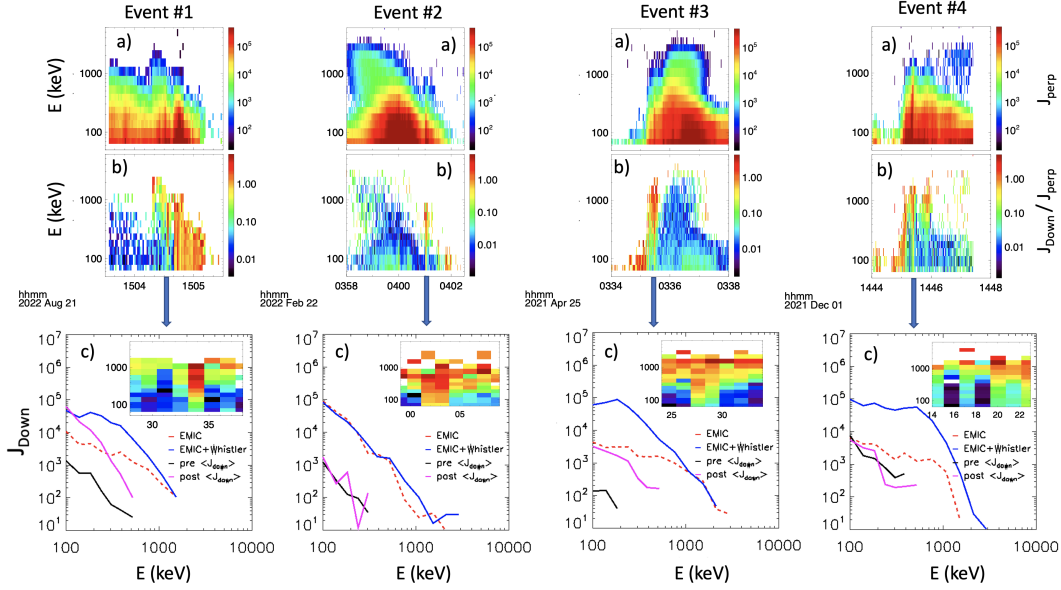


Figure 1. Four events of ELFIN observations of electron precipitation: top panels (a) show locally trapped (i.e., outside the local loss cone, or near-perpendicular) electron fluxes j_{perp} ; middle panels (b) show precipitating (down-going)-to-trapped flux ratio (j_{down}/j_{perp}); bottom panels (c) show energy spectra of precipitating electrons during subintervals (shown by arrow and corresponding panel inserts) with relativistic and subrelativistic electron precipitation bursts exhibiting EMIC-only and EMIC & whistler-mode wave signatures. Bottom panels also include the average background fluxes before (pre $\langle j_{down} \rangle$) and after (post $\langle j_{down} \rangle$) each subinterval.

118 dle panels of Figure 1 show that precipitation events contain both spin-scale bursts with
 119 EMIC-driven precipitation only (j_{down}/j_{perp} maximizing at relativistic energies) and bursts
 120 with combined whistler-mode and EMIC effects (j_{down}/j_{perp} is high over the entire en-
 121 ergy range). Therefore, we may interpret these events as short-time-scale whistler-driven
 122 precipitation bursts embedded within large-time-scale EMIC-driven precipitation. The
 123 scale difference is likely due to the different spatial scales of equatorial generation regions
 124 of EMIC waves (thousands of km, see Blum et al., 2016, 2017; Angelopoulos et al., 2023)
 125 and whistler-mode waves (hundreds of km, see Agapitov et al., 2017). Note that the pre-
 126 cipitating flux levels during precipitation bursts are much higher than the background
 127 precipitating fluxes levels i.e., indeed these observations allow us to compare the efficiency
 128 of EMIC-only versus EMIC and whistler-mode burst-driven precipitation with no con-
 129 tribution from background waves. The bottom panels of Figure 1 demonstrate that in
 130 the presence of whistler-mode waves, not only precipitation of sub-relativistic electrons
 131 ($< 500\text{keV}$) is enhanced, which should be directly scattered by whistler-mode waves,
 132 but precipitation of relativistic electrons (likely scattered by EMIC waves) is also enhanced.

133 3 Event with ELFIN/THEMIS Observations of EMIC and Whistler 134 Waves

135 This section describes an event with ELFIN-A measurements similar to those shown
 136 in Figure 1, but with conjugate, near-equatorial wave measurements by THEMIS. Figure
 137 2 shows the ELFIN-A measurements which were collected on 29 April 2021, at L -
 138 shell ~ 5 near the dawn sector of the southern hemisphere. At $\sim 04:10:40$ UT, precip-
 139 itating (down-going) fluxes (J_{down}) of 300 keV to 2.5 MeV electrons suddenly increase

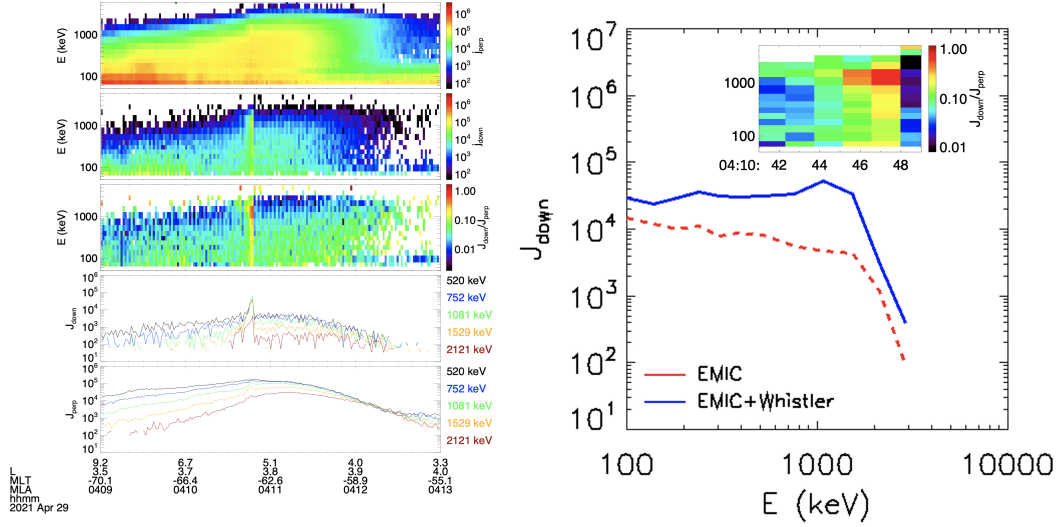


Figure 2. Overview of ELFIN-A observations (left panels): locally trapped fluxes (j_{perp}), precipitating or down-going fluxes (j_{down}), precipitating-to-trapped flux ratio (j_{down}/j_{perp}), 1D spectra j_{down} and j_{perp} at five energy channels (520 keV-2121 keV). L , MLT, and MLAT of ELFIN-A are marked at the bottom. The right panel depicts the average precipitating fluxes as a function of energy due to combined EMIC and whistler-mode waves (solid-blue curve) and EMIC waves only (dashed-red curve) for the sub-interval (as shown by down-to-perpendicular flux ratio inserted spectrogram similar to Figure 1 bottom panels)

140 with the highest precipitating to trapped flux ratio above 1 MeV. The locally trapped
 141 (near-perpendicular) electron fluxes (J_{perp}) show enhancement over a wide range of L -
 142 shells (4-6.5), exhibiting low precipitating to trapped flux ratio (J_{down}/J_{perp} is mostly
 143 less than 0.1) except for a few spins around 04:10:40 UT where this ratio can be greater
 144 than 0.5. The most intense burst of precipitation shows J_{down}/J_{perp} enhancement max-
 145 imizing at relativistic energies ~ 1 MeV (the typical range of EMIC-driven precipitation),
 146 but extending down to 50keV (the typical range of whistler-wave-driven precipitation).
 147 Note that the enhanced relativistic electron precipitation lasts longer than the enhance-
 148 ment of < 500 keV precipitation (which only lasts for a single spin). This is indicative
 149 of a short whistler-mode burst embedded within a large-scale EMIC generation region.

150 During this event, ELFIN magnetically mapped close to the near-equatorial THEMIS-
 151 E spacecraft (Angelopoulos, 2008), which, at the time, was moving from lower L to higher
 152 L , observed the pertinent EMIC and whistler-mode waves and measured the properties
 153 of the cold plasma, and magnetic fields. We use magnetic field data from Flux Gate Mag-
 154 netometer (FGM)(Auster et al., 2008). During fast mode, FGM measures waveforms at
 155 a time resolution of $1/16$ s, sufficient to resolve the EMIC wave frequency range. Mea-
 156 surements of the THEMIS Search Coil Magnetometer (Le Contel et al., 2008) well cover
 157 the whistler-mode frequency range. The cold plasma density is inferred from the space-
 158 craft potential (Nishimura et al., 2013) measured by THEMIS Electric Field Instrument
 159 (Bonnell et al., 2008).

160 Supplementary Figure S1 shows that during this event, THEMIS-E observed whistler-
 161 mode waves around and outside of the plasmopause, identified as a strong plasma fre-
 162 quency (plasma density) gradient. At the plasmopause, THEMIS-E also observed He^+
 163 band EMIC waves (field-aligned, left-hand polarized waves). The ratio of plasma to elec-
 164 tron cyclotron frequency, $f_{pe}/f_{ce,eq}$, varies from ~ 20 to 5 across the plasmopause. Note

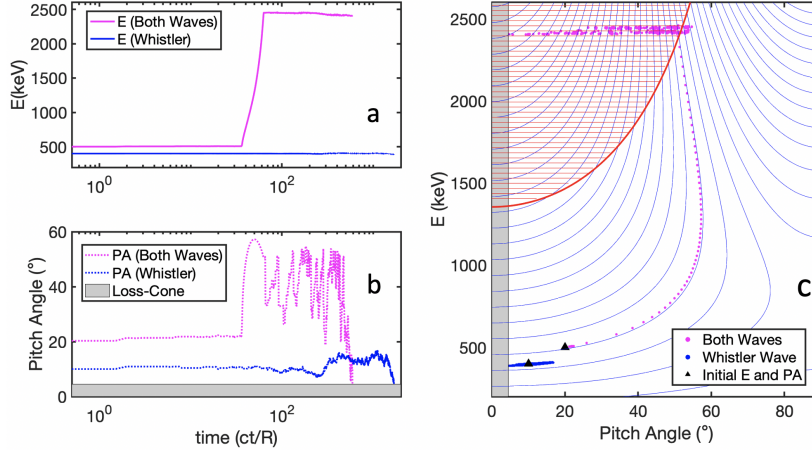


Figure 3. Illustrative electron trajectories from our simulations. Panels (a,b) depict the temporal (in units of ct/LR_E) evolution of the electron’s energy and pitch angle for whistler-mode waves only (blue curve) and for the combined effect (magenta curve) of whistler-mode and EMIC waves. The loss-cone (assumed to be 4.5°) is shaded in grey in Panel (b). Panel (c) shows the same trajectories on an energy, pitch-angle plane, with resonance curves for whistler-mode (blue curves) and EMIC (red lines) waves overlaid, and the range of EMIC resonance energies is shown by a thick red curve. The blue dots show electron trajectory (starting at an initial energy of 400keV and an equatorial pitch angle of 10° , represented by the triangle) directly scattered by whistler waves into loss-cone; the other electron trajectory (magenta dots), with an initial energy of 500 keV and an equatorial pitch angle of 20° , show that the electron gets accelerated by whistler waves and then quickly scattered into loss-cone by EMIC waves.

165 that the projection of ELFIN to the equatorial plane is subject to uncertainties of em-
 166 pirical magnetic field models. Thus, this THEMIS-ELFIN conjunction is only approx-
 167 imate. ELFIN observations of relativistic electron precipitation burst and THEMIS ob-
 168 servations of EMIC waves are within the $\Delta L = \pm 1$, $\Delta MLT = 2$ of each other. These
 169 ranges are comparable to the spatial scale of the typical EMIC wave source region (Blum
 170 et al., 2016, 2017), whereas an ~ 40 min time difference between THEMIS and ELFIN
 171 observations is within the lifetime of EMIC wave source region (Engebretson et al., 2015;
 172 Blum et al., 2020). Whistler mode waves are observed by all three THEMIS probes dur-
 173 ing the entire ~ 2 hour interval within the $\Delta MLT \sim 2$ domain. However, we should
 174 note that the EMIC burst is observed by THEMIS E only, whereas A and D located $\pm 1.5R_E$
 175 away from E do not detect these EMIC bursts. Thus, we cannot exclude the possibil-
 176 ity of a small-scale EMIC source region (e.g., Frey et al., 2004). But ELFIN observations
 177 of relativistic electron precipitation without ~ 50 keV precipitation (two spins before the
 178 main precipitation burst, see the inserted panel in Fig. 2) confirm that there was scat-
 179 tering by equatorial EMIC waves, which may relate to THEMIS-E observations.

180 4 Discussion

181 Figures 1, 2 show that the presence of whistler-mode waves may enhance the precip-
 182 itation of relativistic electrons. One possible mechanism of such enhancement is that
 183 intense whistler-mode waves drive electron acceleration (e.g., turning acceleration, see
 184 Omura et al., 2007; Summers & Omura, 2007), and the accelerated electrons supplement
 185 the population that are to be scattered by EMIC waves (Bashir et al., 2022a). In order
 186 to verify this scenario, we perform simple test particle simulations. The simulation is based

187 on Hamiltonian equations for a monochromatic wave (see Vainchtein et al., 2018; Arte-
 188 myev et al., 2021), and this simplification (constant wave frequency) may reduce the ef-
 189 ficiency of wave-particle resonant interactions (see discussion of frequency drift contri-
 190 bution in Demekhov et al., 2006; Katoh & Omura, 2007; Hiraga & Omura, 2020).

191 We consider the precipitation event of Figure 2, for which we have near-equatorial
 192 observations of waves (see the supplementary information). For the whistler wave, we
 193 use the frequency $f_{wh}/f_{ce,eq} = 0.3$ & 0.4 , the observed wave amplitude at $B_{w,wh} =$
 194 $500 \text{ pT} \cdot \Lambda(\lambda)$, the whistler wave latitudinal profile modeled as $\Lambda(\lambda) = 0.5 \cdot (1 + \tanh(\lambda/\delta\lambda_1)) \exp(-(\lambda/\delta\lambda_2)^2)$
 195 and $\delta\lambda_{1,2} = 1^\circ, 40^\circ$ (e.g., we assume wave generation at the equator and damping at
 196 high latitudes, see details of this empirical wave model in Agapitov et al., 2018). For the
 197 ducted whistler case, we have used $\Lambda(\lambda) \rightarrow 1$. We also include wave field modulation
 198 by assuming whistler-mode waves propagate in wave packets: $B_{w,wh} \rightarrow B_{w,wh} \cdot \Phi(l)$
 199 with $\Phi(l) = \exp(-0.25 \cdot (\sin(\phi/(2\pi l))^2))$, where ϕ is the wave phase and $l = 300$ de-
 200 termines the wave-packet size (we use the longest wave packets from observations, see
 201 statistics in Zhang et al., 2019, 2021).

202 For the He^+ band EMIC wave, we use the most intense wave from observations,
 203 with an amplitude of $B_{w,EMIC} = 500 \text{ pT}$, at a fixed frequency $f_{EMIC}/f_{cp,eq} = 0.2$.
 204 Plasma composition is assumed to be 20% helium and 80% cold protons (Lee et al., 2012;
 205 Lee & Angelopoulos, 2014), and latitudinal distribution of EMIC waves as $B_{w,EMIC} \rightarrow$
 206 $B_{w,EMIC} \cdot \Lambda(\lambda)$ with $\Lambda(\lambda) = 0.5(\tanh(\lambda/\delta\lambda_1) - \tanh((\lambda - \delta\lambda_2)/\delta\lambda_1))$ with $\delta\lambda_{1,2} =$
 207 $1^\circ, 15^\circ$, i.e., there is no EMIC wave around and above the helium resonance latitude that
 208 is around $\sim 25^\circ$ for the selected wave frequency. For this study, we used the field-aligned
 209 cold plasma dispersion relation for both whistler and EMIC waves (Stix, 1962), with $f_{pe}/f_{ce,eq} =$
 210 20 , and $L = 4.5$. The time is normalized to a typical scale $R/c \sim 0.1 \text{ s}$ as $R=4.5 R_E$,
 211 where R_E is the radius of the Earth and c is the speed of light and simulation in time
 212 units is run for 200 seconds (see figure S4 for more details).

213 Figure 3 shows two loss mechanisms of energetic electrons with+ initial pitch-angles
 214 that are not in resonance with EMIC waves: (1) electrons directly scattered into the loss-
 215 cone by whistler-mode waves (blue trajectory) or (2) electrons phase trapped and ac-
 216 celerated by whistler-mode waves to energies sufficiently high for resonance with EMIC
 217 waves, and then scattered into loss-cone by EMIC waves (magenta trajectory). Resonance
 218 with whistler-mode waves moves electrons along the resonance curves (Summers et al.,
 219 1998), and thus we are interested in those that will cross the region (above the E_{min} shown
 220 by thick red curve) of electron resonant interaction with EMIC waves (the latter inter-
 221 actions, primarily resulting in pitch-angle scattering, occur along the thin horizontal red
 222 lines). For moderate electron energies, phase trapping results in energy and pitch-angle
 223 increase (e.g., Bortnik et al., 2008; Vainchtein et al., 2018), and thus resonance curves
 224 move away from the loss-cone. However, when the electron energy reaches $\gamma > f_{ce}/f$,
 225 its pitch-angle starts to decrease during the phase trapping (so-called turning accel-
 226 eration Omura et al., 2007; Bashir et al., 2022a). This effect bends the resonance curves
 227 back toward smaller pitch-angles. It thus allows the accelerated electron to escape from
 228 the trapping at an energy and pitch-angle where resonance with EMIC waves can oc-
 229 cur. Supplementary information provides more examples of such a double resonance ef-
 230 fect (trapping acceleration by whistler-mode waves followed by scattering into the loss-
 231 cone by EMIC waves).

232 The model results suggest the following scenario for the formation of the observed
 233 electron precipitation spectrum: The source size of EMIC waves is usually sufficiently
 234 large (Blum et al., 2016, 2017) to provide relativistic electron precipitation within an \sim
 235 $1R_E$ region near the equator (Capannolo et al., 2019), which corresponds to several spins
 236 of ELFIN observations at low altitudes (see several examples of ELFIN observed EMIC-
 237 driven precipitation in, e.g., Grach et al., 2021; An et al., 2022; Angelopoulos et al., 2023).
 238 Therefore, the relativistic electron precipitation within 04:10:35-04:10:50 UT should be
 239 attributed to EMIC waves. At the beginning of this subinterval, there is no strong sub-

240 MeV precipitation (see j_{prec}/j_{trap} in Figure 2) which we assert is indicative of an ab-
 241 sence of strong whistler-mode waves. We interpret the following burst of < 1 MeV pre-
 242 cipitation around 04:10:45 UT as due to a whistler-mode wave burst (the short duration
 243 of the precipitation burst should be attributed to the small scale of whistler-mode wave
 244 source region near the equator, see Agapitov et al., 2017). This whistler-mode wave burst
 245 is sufficiently strong to provide electron acceleration, and thus efficiently increase > 1 MeV
 246 electron fluxes that are further precipitated by EMIC waves (see an increase of j_{trap} as-
 247 sociated with j_{prec} increase in Figure 2). However, we shall caution that due to large un-
 248 certainties of ELFIN/THEMIS mapping and the time/spatial separation of precipita-
 249 tion events and THEMIS wave measurements, this interpretation is presently a reason-
 250 able hypothesis supported by the limited dataset examined, and needs to be confirmed
 251 by further multi-point and statistical analysis in the future. Moreover, we used a rather
 252 simplified wave model that may not describe all important details of wave-particle non-
 253 linear resonances. Therefore, results shown in Figure 3 should be considered as an in-
 254 dication that the combined whistler-mode and EMIC resonant interactions with electrons
 255 may explain the enhanced relativistic electron precipitation observed in Figures 1, 2; but
 256 much more sophisticated and detailed simulations are needed to confirm this scenario
 257 and assess the overall efficiency of the proposed combined precipitation mechanism.

258 5 Conclusions

259 This letter reports the observation of relativistic electron precipitation driven by
 260 the scattering of EMIC waves with the effect of precipitation enhancement by concu-
 261 rent whistler-mode waves. For five events, ELFIN observed electron precipitation at 300keV-
 262 2.5 MeV, and precipitating fluxes which were higher during subintervals containing both
 263 EMIC and whistler-driven precipitation, compared to subintervals of EMIC-driven pre-
 264 cipitation alone. We propose the scenario of electron acceleration (via the nonlinear res-
 265 onant acceleration, e.g., phase trapping and turning acceleration) by whistler-mode waves
 266 up to relativistic energies and subsequent scattering of this accelerated electron popu-
 267 lation by EMIC waves. Simplified test particle simulations confirm that this scenario in-
 268 deed can work. Our results suggest that nonlinear resonant acceleration (Omura et al.,
 269 2007, 2015) may significantly contribute to electron precipitation events observed at low
 270 altitudes.

271 Acknowledgments

272 A.V.A, X.-J.Z., and M.F.B. acknowledge support from the NASA grants 80NSSC20K1270,
 273 80NSSC23K0403. X.-J. Z. acknowledges support from the NSF grant 2021749. V.A. ac-
 274 knowledges support by NSF grants AGS-1242918, and AGS-2019950.

275 We are grateful to NASA's CubeSat Launch Initiative for ELFIN's successful launch
 276 in the desired orbits. We acknowledge the early support of the ELFIN project by the
 277 AFOSR, under its University Nanosat Program, UNP-8 project, contract FA9453-12-
 278 D-0285, and by the California Space Grant program. We acknowledge the critical con-
 279 tributions of numerous volunteer ELFIN team student members.

280 We also acknowledge NASA contract NAS5-02099 for use of data from the THEMIS
 281 mission. We thank K. H. Glassmeier, U. Auster, and W. Baumjohann for the use of FGM
 282 data provided under the lead of the Technical University of Braunschweig and with fi-
 283 nancial support through the German Ministry for Economy and Technology and the Ger-
 284 man Aerospace Center (DLR) under contract 50 OC 0302.

285 Open Research

286 Fluxes measured by ELFIN are available in ELFIN data archive <https://data.elfin.ucla.edu/>
 287 in CDF format.

288 THEMIS data is available at <http://themis.ssl.berkeley.edu/data/themis>. Data
 289 analysis was done using SPEDAS V4.1 (Angelopoulos et al., 2019). The software can be
 290 downloaded from http://spedas.org/wiki/index.php?title=Downloads_and_Installation

291 References

- 292 Agapitov, O. V., Blum, L. W., Mozer, F. S., Bonnell, J. W., & Wygant, J. (2017,
 293 March). Chorus whistler wave source scales as determined from multipoint
 294 Van Allen Probe measurements. *Geophys. Res. Lett.*, *44*, 2634-2642. doi:
 295 10.1002/2017GL072701
- 296 Agapitov, O. V., Mourenas, D., Artemyev, A. V., Mozer, F. S., Hospodarsky, G.,
 297 Bonnell, J., & Krasnoselskikh, V. (2018, January). Synthetic Empirical
 298 Chorus Wave Model From Combined Van Allen Probes and Cluster Statis-
 299 tics. *Journal of Geophysical Research (Space Physics)*, *123*(1), 297-314. doi:
 300 10.1002/2017JA024843
- 301 An, X., Artemyev, A., Angelopoulos, V., Zhang, X., Mourenas, D., & Bortnik, J.
 302 (2022, September). Nonresonant Scattering of Relativistic Electrons by Elec-
 303 tromagnetic Ion Cyclotron Waves in Earth's Radiation Belts. *Phys. Rev.*
 304 *Lett.*, *129*(13), 135101. doi: 10.1103/PhysRevLett.129.135101
- 305 Angelopoulos, V. (2008, December). The THEMIS Mission. *Space Sci. Rev.*, *141*, 5-
 306 34. doi: 10.1007/s11214-008-9336-1
- 307 Angelopoulos, V., Cruce, P., Drozdov, A., Grimes, E. W., Hatzigeorgiu, N., King,
 308 D. A., ... Schroeder, P. (2019, January). The Space Physics Environ-
 309 ment Data Analysis System (SPEDAS). *Space Sci. Rev.*, *215*, 9. doi:
 310 10.1007/s11214-018-0576-4
- 311 Angelopoulos, V., Tsai, E., Bingley, L., Shaffer, C., Turner, D. L., Runov, A., ...
 312 Zhang, G. Y. (2020, July). The ELFIN Mission. *Space Sci. Rev.*, *216*(5), 103.
 313 doi: 10.1007/s11214-020-00721-7
- 314 Angelopoulos, V., Zhang, X. J., Artemyev, A. V., Mourenas, D., Tsai, E., Wilkins,
 315 C., ... Zarifian, A. (2023). Energetic electron precipitation driven by electro-
 316 magnetic ion cyclotron waves from elfin's low altitude perspective. *Space Sci*
 317 *Rev.*, *219*, 37. doi: <https://doi.org/10.1007/s11214-023-00984-w>
- 318 Artemyev, A. V., Agapitov, O., Mourenas, D., Krasnoselskikh, V., Shastun, V., &
 319 Mozer, F. (2016, April). Oblique Whistler-Mode Waves in the Earth's Inner
 320 Magnetosphere: Energy Distribution, Origins, and Role in Radiation Belt Dy-
 321 namics. *Space Sci. Rev.*, *200*(1-4), 261-355. doi: 10.1007/s11214-016-0252-5
- 322 Artemyev, A. V., Neishtadt, A. I., Vasiliev, A. A., Zhang, X.-J., Mourenas, D.,
 323 & Vainchtein, D. (2021, March). Long-term dynamics driven by res-
 324 onant wave-particle interactions: from Hamiltonian resonance theory to
 325 phase space mapping. *Journal of Plasma Physics*, *87*(2), 835870201. doi:
 326 10.1017/S0022377821000246
- 327 Auster, H. U., Glassmeier, K. H., Magnes, W., Aydogar, O., Baumjohann,
 328 W., Constantinescu, D., ... Wiedemann, M. (2008, December). The
 329 THEMIS Fluxgate Magnetometer. *Space Sci. Rev.*, *141*, 235-264. doi:
 330 10.1007/s11214-008-9365-9
- 331 Bashir, M. F., Artemyev, A., Zhang, X.-J., & Angelopoulos, V. (2022a). Ener-
 332 getic electron precipitation driven by the combined effect of ulf, emic, and
 333 whistler waves. *Journal of Geophysical Research: Space Physics*, *127*(1),
 334 e2021JA029871. doi: <https://doi.org/10.1029/2021JA029871>
- 335 Bashir, M. F., Artemyev, A., Zhang, X.-J., & Angelopoulos, V. (2022b). Hot
 336 plasma effects on electron resonant scattering by electromagnetic ion cyclotron
 337 waves. *Geophysical Research Letters*, *49*(11), e2022GL099229. Retrieved
 338 from [https://agupubs.onlinelibrary.wiley.com/doi/abs/10.1029/](https://agupubs.onlinelibrary.wiley.com/doi/abs/10.1029/2022GL099229)
 339 [2022GL099229](https://doi.org/10.1029/2022GL099229) doi: <https://doi.org/10.1029/2022GL099229>
- 340 Bashir, M. F., & Ilie, R. (2018). A new n+ band of electromagnetic ion cyclotron

- 341 waves in multi-ion cold plasmas. *Geophysical Research Letters*, *45*(19), 10,150-
 342 10,159. Retrieved from [https://agupubs.onlinelibrary.wiley.com/doi/](https://agupubs.onlinelibrary.wiley.com/doi/abs/10.1029/2018GL080280)
 343 [abs/10.1029/2018GL080280](https://agupubs.onlinelibrary.wiley.com/doi/abs/10.1029/2018GL080280) doi: <https://doi.org/10.1029/2018GL080280>
- 344 Bashir, M. F., & Ilie, R. (2021). The first observation of n^+ electromagnetic ion
 345 cyclotron waves. *Journal of Geophysical Research: Space Physics*, *126*(3),
 346 e2020JA028716. doi: <https://doi.org/10.1029/2020JA028716>
- 347 Blum, L. W., Agapitov, O., Bonnell, J. W., Kletzing, C., & Wygant, J. (2016,
 348 May). EMIC wave spatial and coherence scales as determined from multipoint
 349 Van Allen Probe measurements. *Geophys. Res. Lett.*, *43*, 4799-4807. doi:
 350 10.1002/2016GL068799
- 351 Blum, L. W., Bonnell, J. W., Agapitov, O., Paulson, K., & Kletzing, C. (2017,
 352 February). EMIC wave scale size in the inner magnetosphere: Observations
 353 from the dual Van Allen Probes. *Geophys. Res. Lett.*, *44*, 1227-1233. doi:
 354 10.1002/2016GL072316
- 355 Blum, L. W., Halford, A., Millan, R., Bonnell, J. W., Goldstein, J., Usanova, M.,
 356 ... Li, X. (2015, July). Observations of coincident EMIC wave activity and
 357 duskside energetic electron precipitation on 18-19 January 2013. *Geophys.*
 358 *Res. Lett.*, *42*, 5727-5735. doi: 10.1002/2015GL065245
- 359 Blum, L. W., Remya, B., Denton, M. H., & Schiller, Q. (2020, March). Persist-
 360 ent EMIC Wave Activity Across the Nightside Inner Magnetosphere. *Geo-*
 361 *phys. Res. Lett.*, *47*(6), e87009. doi: 10.1029/2020GL087009
- 362 Bonnell, J. W., Mozer, F. S., Delory, G. T., Hull, A. J., Ergun, R. E., Cully, C. M.,
 363 ... Harvey, P. R. (2008, December). The Electric Field Instrument (EFI) for
 364 THEMIS. *Space Sci. Rev.*, *141*, 303-341. doi: 10.1007/s11214-008-9469-2
- 365 Bortnik, J., Thorne, R. M., & Inan, U. S. (2008, November). Nonlinear interac-
 366 tion of energetic electrons with large amplitude chorus. *Geophys. Res. Lett.*,
 367 *35*, 21102. doi: 10.1029/2008GL035500
- 368 Capannolo, L., Li, W., Ma, Q., Shen, X. C., Zhang, X. J., Redmon, R. J., ... Raita,
 369 T. (2019, Apr). Energetic Electron Precipitation: Multievent Analysis of Its
 370 Spatial Extent During EMIC Wave Activity. *Journal of Geophysical Research*
 371 *(Space Physics)*, *124*(4), 2466-2483. doi: 10.1029/2018JA026291
- 372 Capannolo, L., Li, W., Ma, Q., Zhang, X.-J., Redmon, R. J., Rodriguez, J. V., ...
 373 Reeves, G. D. (2018, July). Understanding the Driver of Energetic Electron
 374 Precipitation Using Coordinated Multisatellite Measurements. *Geophys. Res.*
 375 *Lett.*, *45*, 6755-6765. doi: 10.1029/2018GL078604
- 376 Capannolo, L., Li, W., Millan, R., Smith, D., Sivadas, N., Sample, J., & Shekhar,
 377 S. (2022). Relativistic electron precipitation near midnight: Drivers, distribu-
 378 tion, and properties. *Journal of Geophysical Research (Space Physics)*, *127*,
 379 e2021JA030111. doi: 10.1029/2021JA030111
- 380 Demekhov, A. G., Trakhtengerts, V. Y., Rycroft, M. J., & Nunn, D. (2006, Decem-
 381 ber). Electron acceleration in the magnetosphere by whistler-mode waves
 382 of varying frequency. *Geomagnetism and Aeronomy*, *46*, 711-716. doi:
 383 10.1134/S0016793206060053
- 384 Drozdov, A. Y., Usanova, M. E., Hudson, M. K., Allison, H. J., & Shprits, Y. Y.
 385 (2020, September). The Role of Hiss, Chorus, and EMIC Waves in the
 386 Modeling of the Dynamics of the Multi-MeV Radiation Belt Electrons.
 387 *Journal of Geophysical Research (Space Physics)*, *125*(9), e28282. doi:
 388 10.1029/2020JA028282
- 389 Engebretson, M. J., Posch, J. L., Wygant, J. R., Kletzing, C. A., Lessard, M. R.,
 390 Huang, C.-L., ... Shiokawa, K. (2015, July). Van Allen probes, NOAA,
 391 GOES, and ground observations of an intense EMIC wave event extending
 392 over 12 h in magnetic local time. *J. Geophys. Res.*, *120*, 5465-5488. doi:
 393 10.1002/2015JA021227
- 394 Frey, H. U., Haerendel, G., Mende, S. B., Forrester, W. T., Immel, T. J., &
 395 ØStgaard, N. (2004, October). Subauroral morning proton spots (SAMPS)

- 396 as a result of plasmopause-ring-current interaction. *Journal of Geophysical*
 397 *Research (Space Physics)*, 109(A10), A10305. doi: 10.1029/2004JA010516
- 398 Glauert, S. A., & Horne, R. B. (2005, April). Calculation of pitch angle and energy
 399 diffusion coefficients with the PADIE code. *J. Geophys. Res.*, 110, 4206. doi:
 400 10.1029/2004JA010851
- 401 Grach, V. S., Artemyev, A. V., Demekhov, A. G., Zhang, X.-J., Bortnik, J., An-
 402 gelopoulos, V., ... Roberts, O. W. (2022, September). Relativistic Electron
 403 Precipitation by EMIC Waves: Importance of Nonlinear Resonant Effects.
 404 *Geophys. Res. Lett.*, 49(17), e99994. doi: 10.1029/2022GL099994
- 405 Grach, V. S., & Demekhov, A. G. (2020, February). Precipitation of Relativistic
 406 Electrons Under Resonant Interaction With Electromagnetic Ion Cyclotron
 407 Wave Packets. *Journal of Geophysical Research (Space Physics)*, 125(2),
 408 e27358. doi: 10.1029/2019JA027358
- 409 Grach, V. S., Demekhov, A. G., & Larchenko, A. V. (2021, December). Res-
 410 onant interaction of relativistic electrons with realistic electromagnetic
 411 ion-cyclotron wave packets. *Earth, Planets and Space*, 73(1), 129. doi:
 412 10.1186/s40623-021-01453-w
- 413 Hiraga, R., & Omura, Y. (2020, February). Acceleration mechanism of radiation belt
 414 electrons through interaction with multi-subpacket chorus waves. *Earth, Plan-*
 415 *ets, and Space*, 72(1), 21. doi: 10.1186/s40623-020-1134-3
- 416 Hsieh, Y.-K., Kubota, Y., & Omura, Y. (2020). Nonlinear evolution of radiation
 417 belt electron fluxes interacting with oblique whistler mode chorus emissions.
 418 *Journal of Geophysical Research: Space Physics*, e2019JA027465. Retrieved
 419 from [https://agupubs.onlinelibrary.wiley.com/doi/abs/10.1029/](https://agupubs.onlinelibrary.wiley.com/doi/abs/10.1029/2019JA027465)
 420 [2019JA027465](https://agupubs.onlinelibrary.wiley.com/doi/abs/10.1029/2019JA027465) (e2019JA027465 2019JA027465) doi: 10.1029/2019JA027465
- 421 Hsieh, Y.-K., & Omura, Y. (2017, January). Nonlinear dynamics of electrons inter-
 422 acting with oblique whistler mode chorus in the magnetosphere. *J. Geophys.*
 423 *Res.*, 122, 675-694. doi: 10.1002/2016JA023255
- 424 Katoh, Y., & Omura, Y. (2007, July). Relativistic particle acceleration in the
 425 process of whistler-mode chorus wave generation. *Geophys. Res. Lett.*, 34,
 426 L13102. doi: 10.1029/2007GL029758
- 427 Kersten, T., Horne, R. B., Glauert, S. A., Meredith, N. P., Fraser, B. J., & Grew,
 428 R. S. (2014, November). Electron losses from the radiation belts caused by
 429 EMIC waves. *J. Geophys. Res.*, 119, 8820-8837. doi: 10.1002/2014JA020366
- 430 Le Contel, O., Roux, A., Robert, P., Coillot, C., Bouabdellah, A., de La Porte,
 431 B., ... Larson, D. (2008, December). First Results of the THEMIS
 432 Search Coil Magnetometers. *Space Sci. Rev.*, 141, 509-534. doi: 10.1007/
 433 s11214-008-9371-y
- 434 Lee, J. H., & Angelopoulos, V. (2014, Mar). On the presence and properties of cold
 435 ions near Earth's equatorial magnetosphere. *Journal of Geophysical Research*
 436 *(Space Physics)*, 119(3), 1749-1770. doi: 10.1002/2013JA019305
- 437 Lee, J. H., Chen, L., Angelopoulos, V., & Thorne, R. M. (2012, Jun). THEMIS
 438 observations and modeling of multiple ion species and EMIC waves: Implica-
 439 tions for a vanishing He⁺ stop band. *Journal of Geophysical Research (Space*
 440 *Physics)*, 117(A6), A06204. doi: 10.1029/2012JA017539
- 441 Li, W., & Hudson, M. K. (2019, Nov). Earth's Van Allen Radiation Belts: From
 442 Discovery to the Van Allen Probes Era. *Journal of Geophysical Research*
 443 *(Space Physics)*, 124(11), 8319-8351. doi: 10.1029/2018JA025940
- 444 Millan, R. M., & Thorne, R. M. (2007, March). Review of radiation belt relativistic
 445 electron losses. *Journal of Atmospheric and Solar-Terrestrial Physics*, 69, 362-
 446 377. doi: 10.1016/j.jastp.2006.06.019
- 447 Mourenas, D., Artemyev, A. V., Ma, Q., Agapitov, O. V., & Li, W. (2016, May).
 448 Fast dropouts of multi-MeV electrons due to combined effects of EMIC
 449 and whistler mode waves. *Geophys. Res. Lett.*, 43(9), 4155-4163. doi:
 450 10.1002/2016GL068921

- 451 Ni, B., Cao, X., Zou, Z., Zhou, C., Gu, X., Bortnik, J., ... Xie, L. (2015, Septem-
 452 ber). Resonant scattering of outer zone relativistic electrons by multiband
 453 EMIC waves and resultant electron loss time scales. *J. Geophys. Res.*, *120*,
 454 7357-7373. doi: 10.1002/2015JA021466
- 455 Ni, B., Thorne, R. M., & Ma, Q. (2012, April). Bounce-averaged Fokker-
 456 Planck diffusion equation in non-dipolar magnetic fields with applications
 457 to the Dungey magnetosphere. *Annales Geophysicae*, *30*, 733-750. doi:
 458 10.5194/angeo-30-733-2012
- 459 Ni, B., Thorne, R. M., Zhang, X., Bortnik, J., Pu, Z., Xie, L., ... Gu, X. (2016,
 460 April). Origins of the Earth's Diffuse Auroral Precipitation. *Space Sci. Rev.*,
 461 *200*, 205-259. doi: 10.1007/s11214-016-0234-7
- 462 Nishimura, Y., Bortnik, J., Li, W., Thorne, R. M., Ni, B., Lyons, L. R., ... Auster,
 463 U. (2013, Feb). Structures of dayside whistler-mode waves deduced from
 464 conjugate diffuse aurora. *Journal of Geophysical Research (Space Physics)*,
 465 *118*(2), 664-673. doi: 10.1029/2012JA018242
- 466 Omura, Y., Furuya, N., & Summers, D. (2007, June). Relativistic turning ac-
 467 celeration of resonant electrons by coherent whistler mode waves in a dipole
 468 magnetic field. *J. Geophys. Res.*, *112*, 6236. doi: 10.1029/2006JA012243
- 469 Omura, Y., Miyashita, Y., Yoshikawa, M., Summers, D., Hikishima, M., Ebihara, Y.,
 470 & Kubota, Y. (2015, November). Formation process of relativistic electron flux
 471 through interaction with chorus emissions in the Earth's inner magnetosphere.
 472 *J. Geophys. Res.*, *120*, 9545-9562. doi: 10.1002/2015JA021563
- 473 Shprits, Y. Y., Drozdov, A. Y., Spasojevic, M., Kellerman, A. C., Usanova, M. E.,
 474 Engebretson, M. J., ... Aseev, N. A. (2016, September). Wave-induced loss of
 475 ultra-relativistic electrons in the Van Allen radiation belts. *Nature Communi-
 476 cations*, *7*, 12883. doi: 10.1038/ncomms12883
- 477 Shprits, Y. Y., Kellerman, A., Aseev, N., Drozdov, A. Y., & Michaelis, I. (2017,
 478 Feb). Multi-MeV electron loss in the heart of the radiation belts. *Geophys.
 479 Res. Lett.*, *44*(3), 1204-1209. doi: 10.1002/2016GL072258
- 480 Shprits, Y. Y., Subbotin, D. A., Meredith, N. P., & Elkington, S. R. (2008, Novem-
 481 ber). Review of modeling of losses and sources of relativistic electrons in the
 482 outer radiation belt II: Local acceleration and loss. *Journal of Atmospheric
 483 and Solar-Terrestrial Physics*, *70*, 1694-1713. doi: 10.1016/j.jastp.2008.06.014
- 484 Stix, T. H. (1962). *The Theory of Plasma Waves*.
- 485 Summers, D. (2005, August). Quasi-linear diffusion coefficients for field-aligned elec-
 486 tromagnetic waves with applications to the magnetosphere. *J. Geophys. Res.*,
 487 *110*, 8213. doi: 10.1029/2005JA011159
- 488 Summers, D., Ni, B., & Meredith, N. P. (2007a, April). Timescales for radiation
 489 belt electron acceleration and loss due to resonant wave-particle interactions:
 490 1. Theory. *J. Geophys. Res.*, *112*, 4206. doi: 10.1029/2006JA011801
- 491 Summers, D., Ni, B., & Meredith, N. P. (2007b, April). Timescales for radiation belt
 492 electron acceleration and loss due to resonant wave-particle interactions: 2.
 493 Evaluation for VLF chorus, ELF hiss, and electromagnetic ion cyclotron waves.
 494 *J. Geophys. Res.*, *112*, 4207. doi: 10.1029/2006JA011993
- 495 Summers, D., & Omura, Y. (2007, December). Ultra-relativistic acceleration of elec-
 496 trons in planetary magnetospheres. *Geophys. Res. Lett.*, *34*, 24205. doi: 10
 497 .1029/2007GL032226
- 498 Summers, D., & Thorne, R. M. (2003, April). Relativistic electron pitch-angle scat-
 499 tering by electromagnetic ion cyclotron waves during geomagnetic storms. *J.
 500 Geophys. Res.*, *108*, 1143. doi: 10.1029/2002JA009489
- 501 Summers, D., Thorne, R. M., & Xiao, F. (1998, September). Relativistic theo-
 502 ry of wave-particle resonant diffusion with application to electron accel-
 503 eration in the magnetosphere. *J. Geophys. Res.*, *103*, 20487-20500. doi:
 504 10.1029/98JA01740
- 505 Thorne, R. M., Bortnik, J., Li, W., & Ma, Q. (2021). Wave-particle interactions

- 506 in the earth's magnetosphere. In *Magnetospheres in the solar system* (p. 93-
 507 108). American Geophysical Union (AGU). doi: [https://doi.org/10.1002/](https://doi.org/10.1002/9781119815624.ch6)
 508 [9781119815624.ch6](https://doi.org/10.1002/9781119815624.ch6)
- 509 Tsai, E., Artemyev, A., Zhang, X.-J., & Angelopoulos, V. (2022, May). Relativistic
 510 Electron Precipitation Driven by Nonlinear Resonance With Whistler-Mode
 511 Waves. *Journal of Geophysical Research (Space Physics)*, *127*(5), e30338. doi:
 512 [10.1029/2022JA030338](https://doi.org/10.1029/2022JA030338)
- 513 Usanova, M. E., Drozdov, A., Orlova, K., Mann, I. R., Shprits, Y., Robertson,
 514 M. T., ... Wygant, J. (2014, March). Effect of EMIC waves on relativistic and
 515 ultrarelativistic electron populations: Ground-based and Van Allen Probes ob-
 516 servations. *Geophys. Res. Lett.*, *41*, 1375-1381. doi: [10.1002/2013GL059024](https://doi.org/10.1002/2013GL059024)
- 517 Vainchtein, D., Zhang, X. J., Artemyev, A. V., Mourenas, D., Angelopoulos, V.,
 518 & Thorne, R. M. (2018, October). Evolution of Electron Distribution
 519 Driven by Nonlinear Resonances With Intense Field-Aligned Chorus Waves.
 520 *Journal of Geophysical Research (Space Physics)*, *123*(10), 8149-8169. doi:
 521 [10.1029/2018JA025654](https://doi.org/10.1029/2018JA025654)
- 522 Zhang, X.-J., Angelopoulos, V., Mourenas, D., Artemyev, A., Tsai, E., & Wilkins,
 523 C. (2022, May). Characteristics of Electron Microburst Precipitation Based
 524 on High-Resolution ELFIN Measurements. *Journal of Geophysical Research*
 525 *(Space Physics)*, *127*(5), e30509. doi: [10.1029/2022JA030509](https://doi.org/10.1029/2022JA030509)
- 526 Zhang, X. J., Demekhov, A. G., Katoh, Y., Nunn, D., Tao, X., Mourenas, D.,
 527 ... Angelopoulos, V. (2021, August). Fine Structure of Chorus Wave
 528 Packets: Comparison Between Observations and Wave Generation Mod-
 529 els. *Journal of Geophysical Research (Space Physics)*, *126*(8), e29330. doi:
 530 [10.1029/2021JA029330](https://doi.org/10.1029/2021JA029330)
- 531 Zhang, X. J., Mourenas, D., Artemyev, A. V., Angelopoulos, V., Bortnik, J.,
 532 Thorne, R. M., ... Hospodarsky, G. B. (2019, July). Nonlinear Electron
 533 Interaction With Intense Chorus Waves: Statistics of Occurrence Rates. *Geo-*
 534 *phys. Res. Lett.*, *46*(13), 7182-7190. doi: [10.1029/2019GL083833](https://doi.org/10.1029/2019GL083833)
- 535 Zhang, X.-J., Mourenas, D., Artemyev, A. V., Angelopoulos, V., & Thorne, R. M.
 536 (2017, August). Contemporaneous EMIC and whistler mode waves: Obser-
 537 vations and consequences for MeV electron loss. *Geophys. Res. Lett.*, *44*,
 538 8113-8121. doi: [10.1002/2017GL073886](https://doi.org/10.1002/2017GL073886)

Figure 1.

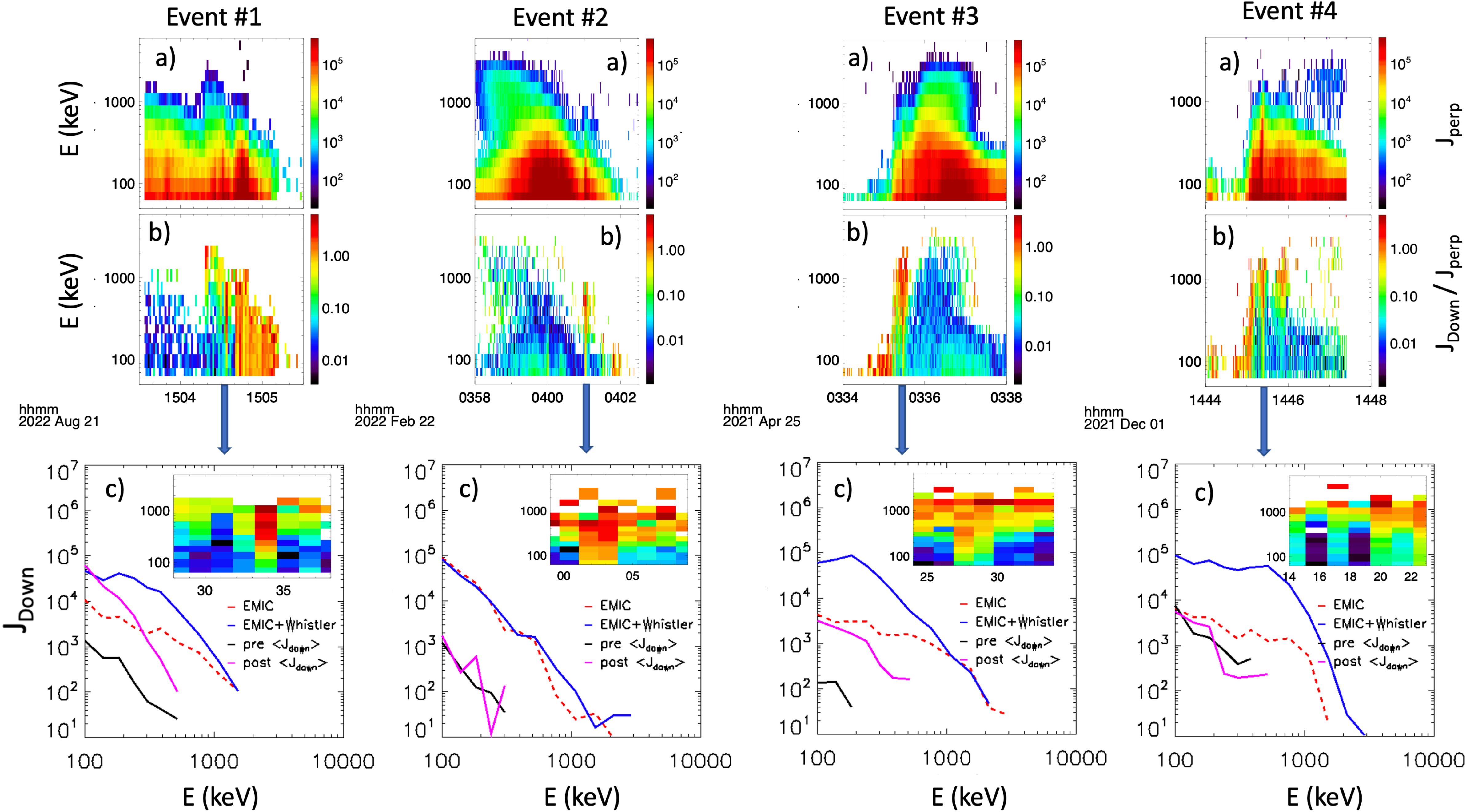


Figure 2.

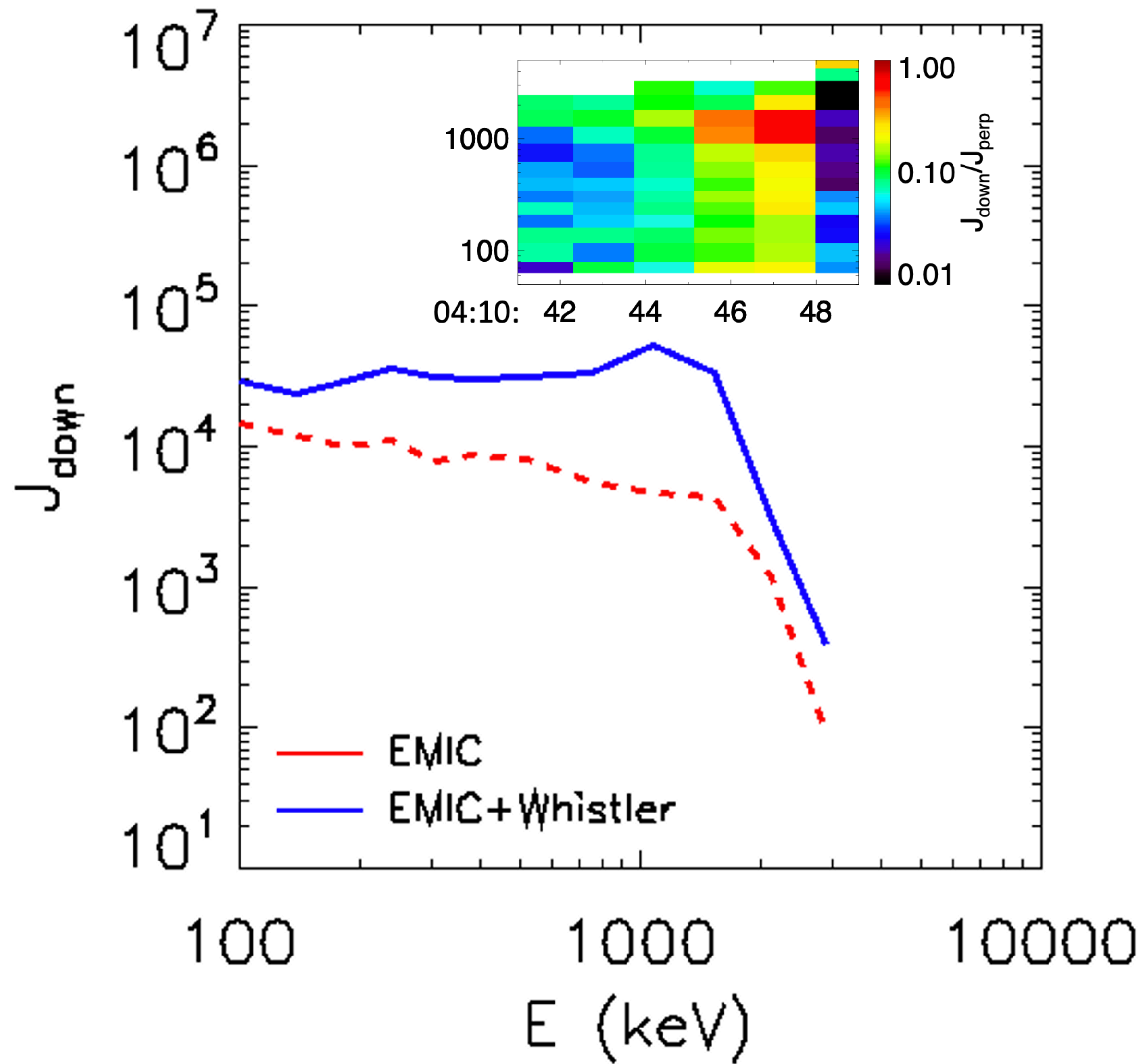
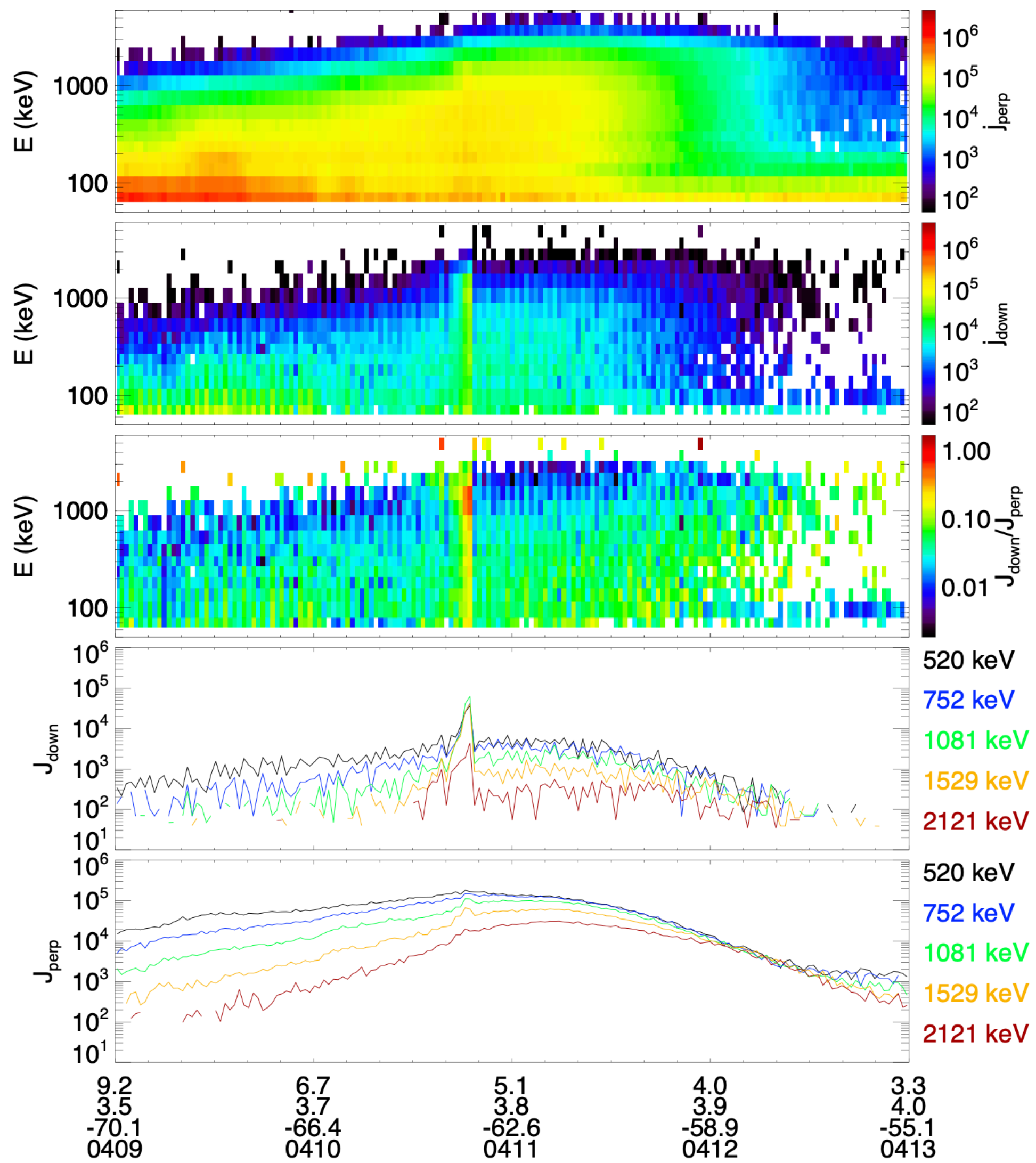


Figure 3.

